JOURNAL OF MATERIALS SCIENCE 37 (2002) 1055–1060

Thermal diffusivity measurement of Zn, Ba, V, Y and Sn doped Bi-Pb-Sr-Ca-Cu-O ceramics superconductors by photoacoustic technique

W. M. M. YUNUS*, C. Y. J. FANNY, T. E. PHING, S. B. MOHAMED, S. A. HALIM, M. M. MOKSIN
Department of Physics, Faculty of Science and Environmental Studies, Universiti Putra Malaysia, 43400 UPM, Serdang, Malaysia
E-mail: mahmood@fsas.upm.edu.my

The simple open photoacoustic cell technique is demonstrated for measuring the thermal diffusivity of the Zn, Ba, V, Y and Sn doped Bi-Pb-Sr-Ca-Cu-O superconducting ceramic samples. It is based upon the measurement of the photoacoustic signal as a function of the modulation frequency in the region where the sample thickness, l_s, equal to the thermal diffusion length of the sample, μ_s. The obtained thermal diffusivity values of Ba, V, Y and Sn doped in Bi-Pb-Sr-Ca-Cu-O system increase with the increasing dopant concentration at Ca side. However, the thermal diffusivity values of Zn doped sample decrease with the increasing of dopant concentration in the system. The measured thermal diffusivity value was found to be very dependent on the dopant atom and dopant concentration.

1. Introduction

After the discovery the formation of the high Tc phase (2223) in Bi-Pb-Sr-Ca-Cu-O system, intensive experimental work has been done by many researchers to enhance the Tc value by addition of dopant in the system [1–3]. However, there seems to exist no systematic investigation of the thermal properties of the system in the literature. In this paper, we describe the use of the open photoacoustic cell (OPC) technique to obtain the thermal diffusivity of $Bi_2Pb_{0.6}Sr_2Ca_{2-x}M_xCu_3O_\delta$, (where M = Zn, Ba, V, Y and Sn and $x = 0.02$–0.10) superconducting ceramic.

The theory of the photoacoustic effect in solid was first described by Rosencwaig and Gersho [4]. Applying the simple one dimensional thermal diffusion model of RG, the pressure fluctuation, P_{th} in the air chamber of the open photoacoustic cell detection given by [5–8]

$$P_{th} = \frac{\gamma P_o I_o (\alpha_g \alpha_s)^{1/2}}{2\pi l_g T_o k_s f} \frac{e^{j(\omega t - \pi/2)}}{\sinh(l_s \sigma_s)} \quad (1)$$

where γ is the air specific heat ratio, $P_o(T_o)$ are the ambient pressure (temperature), I_o is the absorbed light intensity, f is the modulation frequency, l_i, k_i and α_i are the length, thermal conductivity and thermal diffusivity of material i, respectively. The subscript i denotes the sample (s) and gas (g) media. Besides that, $\sigma_i = (1+j)a_i$ and $a_i = (\pi f/\alpha_i)^{1/2}$, is the complex thermal diffusion coefficient of material i. According to this model, the heat generated in the sample will diffuse from the sample to the gas in immediate contact with the sample. In this process, an important parameter involved is the diffusion length of the sample μ_s, which can be defined in terms of the thermal diffusivity by [9]

$$\mu_s = \sqrt{\alpha/(\pi f)} \quad (2)$$

It meant that, μ_s decreases with the increasing modulation frequency. At very low frequency ($f < f_c$) or $\mu_s > l_s$ for the thermally thin sample, the amplitude of the photoacoustic (PA) signal decreases as $f^{-1.5}$ one increases the modulation frequency. In contrast, at high modulation frequencies ($f > f_c$) or $\mu_s < l_s$ for a thermally thick sample, the amplitude of PA signal decreases exponentially with the modulation frequency as $(1/f)\exp(-a\sqrt{f})$, where a, is a parameter defined as $a = l_s\sqrt{\pi/\alpha_s}$. For a characteristic frequency, say $f = f_c$ when the diffusion length becomes equal to sample thickness. The thermal diffusivity can then be calculated by applying the Equation 2 which correspond to the situation $l_s = \mu_s$, one has [10, 11]

$$\alpha_s = \pi f_c l_s^2 \quad (3)$$

The three phenomena considered in this technique is schematically displayed in Fig. 1. However, for a plate shaped solid samples surrounded by the air, the thermoelastic bending of the sample cannot be neglected. This effect is essentially due to the temperature gradient

*Author to whom all correspondence should be addressed.

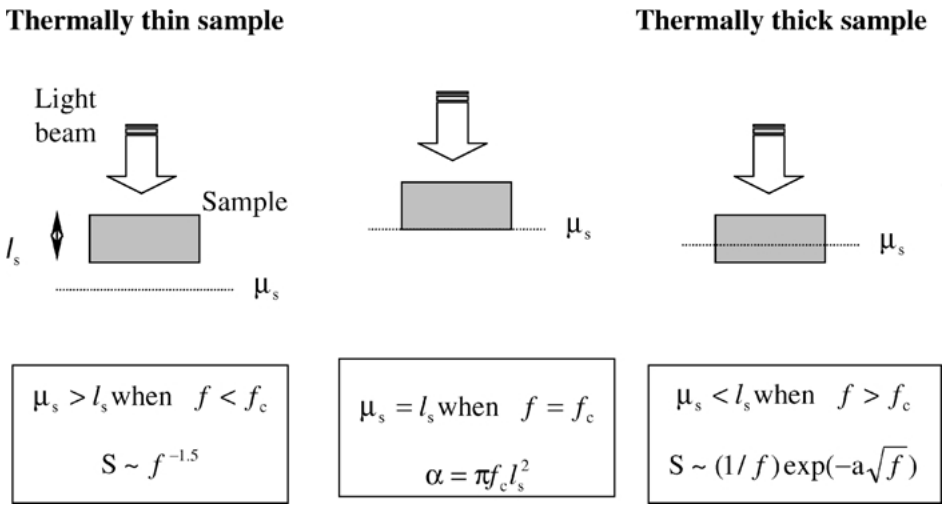

Figure 1 Summary of three phenomena considered in present Open Photoacoustic Cell (OPC) technique.

inside the sample along the thickness axis. This temperature gradient caused displacement along the radial direction of the sample and induces a bending along the sample thickness axis (drum effect). This has been demonstrated by Perondi and Miranda [12] where the PA signal becomes f^{-1} dependence for a thermally thick sample.

2. Experimental procedure

The superconducting ceramic samples of $Bi_2Pb_{0.6}Sr_2Ca_{2-x}Zn_xCu_3O_\delta$ ($x = 0.02$–0.10), $Bi_2Pb_{0.6}Sr_2Ca_{2-x}Ba_xCu_3O_\delta$ ($x = 0.02$–0.10), $Bi_2Pb_{0.6}Sr_2Ca_{2-x}V_xCu_3O_\delta$ ($x = 0.05$–0.10), $Bi_2Pb_{0.6}Sr_2Ca_{2-x}Y_xCu_3O_\delta$ ($x = 0.02$–0.10) and $Bi_2Pb_{0.6}Sr_2Ca_{2-x}Sn_xCu_3O_\delta$ ($x = 0.05$–0.10) were prepared from a mixtures of high purity (99.9%) Bi_2O_3, PbO, $SrCO_3$, $CaCO_3$, M′ (M′ ≡ ZnO_2, $BaCO_3$, V_2O_5, Y_2O_3 or SnO_2) and CuO powders. Firstly, the powders were ball-milled for 24 hours. Then, the mixture was first calcined at 800°C for 24 hours and the second calcination was done at 830°C for 14 hours with intermediate grindings in order to ensure the homogeneity. The mixture was pressed into pellets and sintered at 855°C for 150 hours. The resulting materials were all crystal-like black pellets. After polishing, the thickness of these samples was between 0.44 mm and 0.90 mm as summaries in Table I.

The experimental set up of the OPC configuration is shown in Fig. 2. It consists of mounting the pallet-shaped sample directly onto an electret microphone (Cirkit product, UK) with a circular hole of 2.5 mm diameter by employing silicon grease. Thus, the sample and the microphone diaphragm will form a small photoacoustic cell with the air volume is 7.85 mm^3. The argon-ion laser (Omnichrome 543) beam, which after being mechanically chopped by an optical chopper (Standford Research System SR540) was focused onto the sample. As a result of the periodic heating of the sample by absorption of the modulated light, the heat generated in the sample is transferred to the gas in contact. Hence, the pressure in the air chamber oscillates at the chopping frequency which can be detected by the sensitive microphone. The photoacoustic signal being generated was then amplified by the preamplifier and further analyzed by using the lock-in amplifier. The photoacoustic signal amplitude is recorded as a function of the modulation frequency. All of our measurements were carried out at room temperature.

The electrical resistance of the superconducting ceramic samples was measured in the temperature range of 20 K–300 K by using four-point probe technique. However, the surface morphology and crystal plane of the samples were investigated by using scanning electron microscope, SEM (JEOL model 6400) and

TABLE I The samples thickness and thermal diffusivity values of $Bi_2Pb_{0.6}Sr_2Ca_{2-x}Zn_xCu_3O_\delta$ ($x = 0.02$–0.10), $Bi_2Pb_{0.6}Sr_2Ca_{2-x}Ba_xCu_3O_\delta$ ($x = 0.02$–0.10), $Bi_2Pb_{0.6}Sr_2Ca_{2-x}V_xCu_3O_\delta$ ($x = 0.05$–0.10), $Bi_2Pb_{0.6}Sr_2Ca_{2-x}Y_xCu_3O_\delta$ ($x = 0.02$–0.10) and $Bi_2Pb_{0.6}Sr_2Ca_{2-x}Sn_xCu_3O_\delta$ ($x = 0.05$–0.10)

Dopant	Zn		Ba		V		Y		Sn	
M x	l_s (cm)	α (cm^2/s)	l_s (cm)	α (cm^2/s)	l_s (cm)	α (cm^2/s)	l_s (cm)	α (cm^2/s)	l_s (cm)	α (cm^2/s)
0.02	0.56	0.59	0.44	0.22	–	–	0.50	0.22	–	–
0.04	0.66	0.57	0.76	0.57	–	–	0.51	0.23	–	–
0.05	0.72	0.51	0.44	0.62	0.48	0.24	0.50	0.24	0.46	0.19
0.06	0.71	0.46	0.78	0.68	0.58	0.26	0.57	0.26	0.45	0.20
0.07	0.62	0.41	0.66	0.72	0.58	0.27	0.51	0.28	0.54	0.22
0.08	0.66	0.37	0.73	0.79	0.52	0.28	0.54	0.31	0.45	0.24
0.09	0.55	0.34	0.85	0.85	0.53	0.30	0.50	0.33	0.52	0.30
0.10	0.47	0.23	0.90	1.09	0.49	0.32	0.52	0.30	0.50	0.34

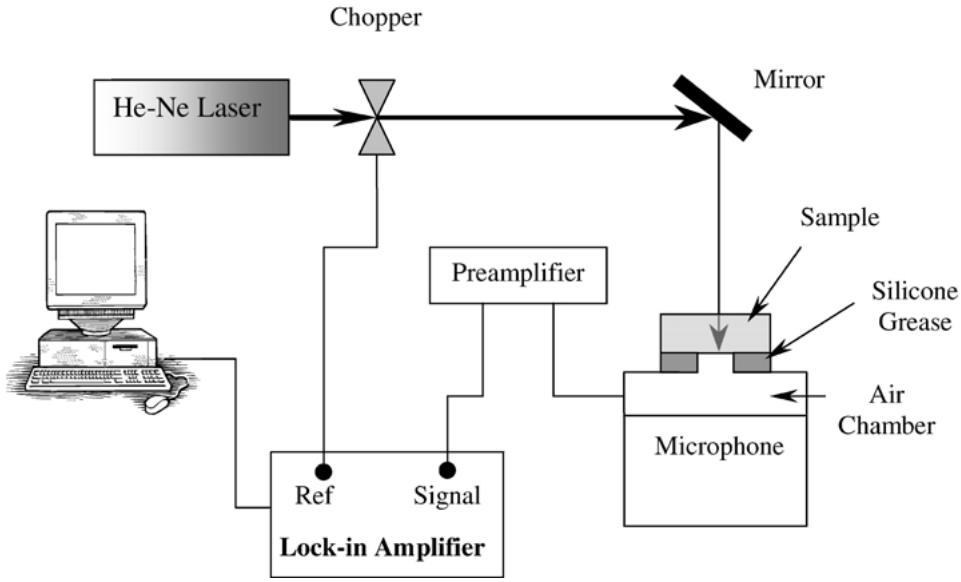

Figure 2 Experimental set-up for Open Photoacoustic Cell (OPC) technique.

X-Ray diffractometer, XRD (Siemens model D-5000) respectively.

3. Results and discussion

By using the analysis method proposed by Costa and Siqueira [13], we plot the *ln* (PA signal) versus *ln* $(\sqrt{f})$ for 0.47 mm thick $Bi_2Pb_{0.6}Sr_2Ca_{2-x}Zn_xCu_3O_\delta$ $(x = 0.1)$ sample as shown in Fig. 3. The characteristic frequency, f_c (frequency at which the sample changes its behavior from thermally thick to thermally thin) was determined to be 32.63 Hz. The thermal diffusivity of this sample was then calculated as 0.23 cm^2/s by using Equation 3. The same procedure was used for the other superconductor composition and the measured thermal diffusivity values of all of our samples are listed in Table I.

The result for the thermal diffusivity as a function of the composition parameter x for $Bi_2Pb_{0.6}Sr_2Ca_{2-x}Zn_x$

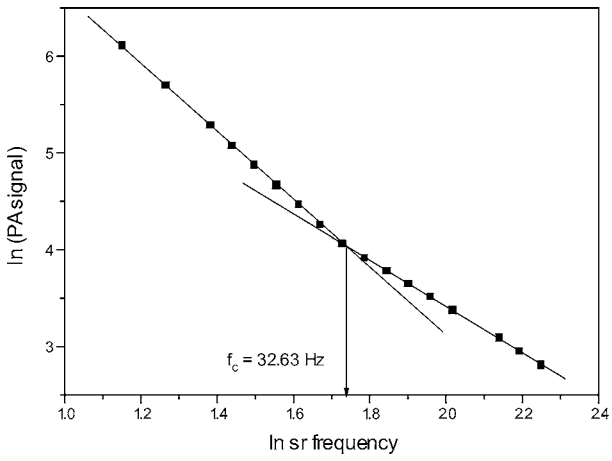

Figure 3 Plot *ln* (PA signal) versus *ln* $(\sqrt{f})$ for 0.47 mm thick $Bi_2Pb_{0.6}Sr_2Ca_{2-x}Zn_xCu_3O_\delta$ $(x = 0.1)$ sample.

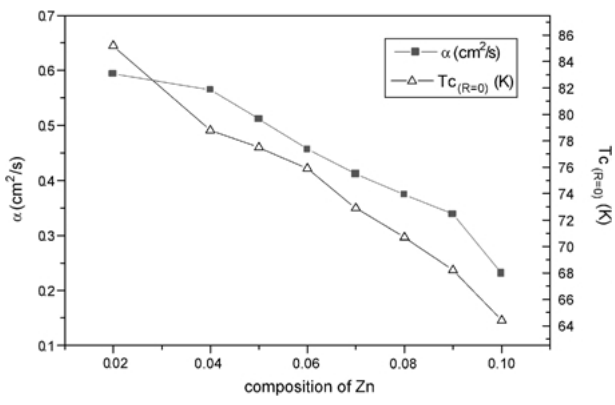

Figure 4 Thermal diffusivity and Tc values versus composition of Zn for $Bi_2Pb_{0.6}Sr_2Ca_{2-x}Zn_xCu_3O_\delta$ $(x = 0.02$–$0.10)$ samples.

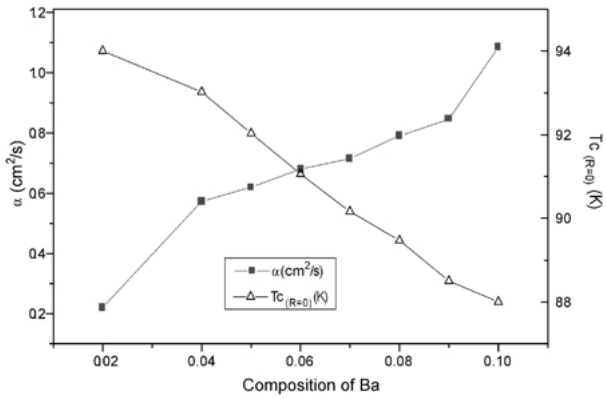

Figure 5 Thermal diffusivity and Tc values versus composition of Ba for $Bi_2Pb_{0.6}Sr_2Ca_{2-x}Ba_xCu_3O_\delta$ $(x = 0.02$–$0.10)$ samples.

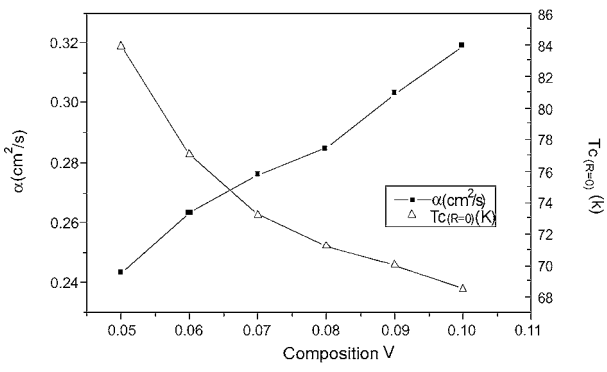

Figure 6 Thermal diffusivity and Tc values versus composition of V for $Bi_2Pb_{0.6}Sr_2Ca_{2-x}V_xCu_3O_\delta$ $(x = 0.05$–$0.10)$ samples.

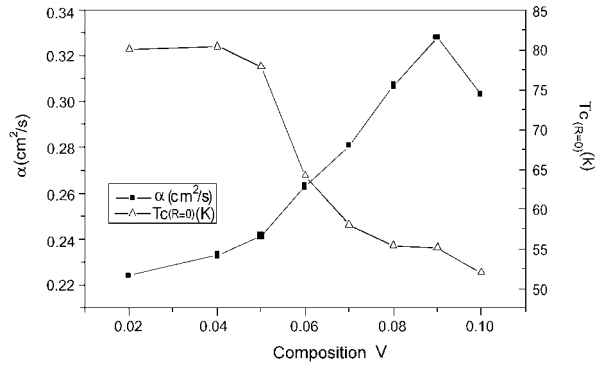

Figure 7 Thermal diffusivity and Tc values versus composition of Y for $Bi_2Pb_{0.6}Sr_2Ca_{2-x}Y_xCu_3O_\delta$ ($x = 0.02$–0.10) samples.

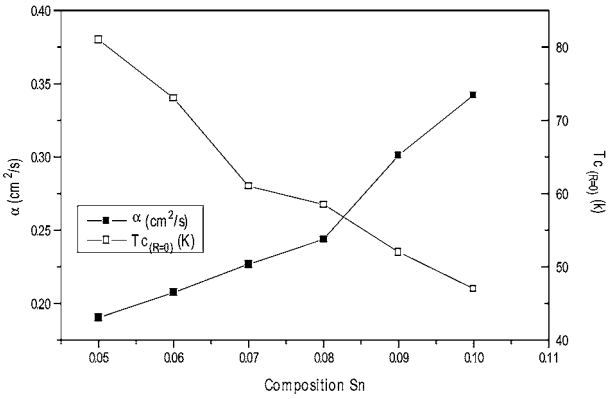

Figure 8 Thermal diffusivity and Tc values versus composition of Sn for $Bi_2Pb_{0.6}Sr_2Ca_{2-x}Y_xCu_3O_\delta$ ($x = 0.05$–0.10) samples.

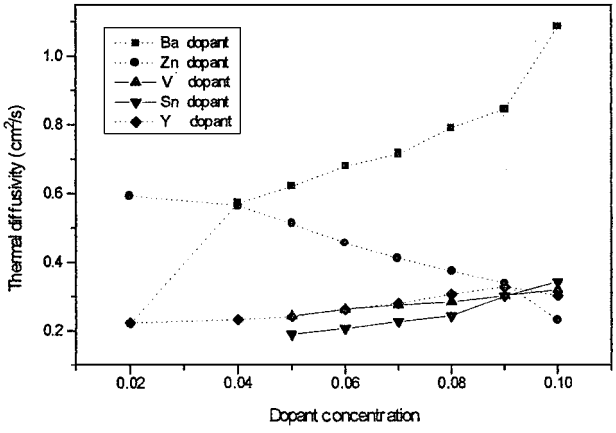

Figure 9 Thermal diffusivity as a function of dopant concentration for $Bi_2Pb_{0.6}Sr_2Ca_{2-x}M_xCu_3O_\delta$ ($x = 0.05$–0.10, M = Zn, Ba, V, Y and Sn) samples.

Cu_3O_δ ($x = 0.02$–0.10) sample is shown in Fig. 4. The thermal diffusivity values decrease with increasing mole fraction x of Zn, where the obtained values drop form 0.59 cm^2/s for $x = 0.02$ to 0.23 cm^2/s for $x = 0.10$. Similarly, the value of $Tc_{(R=0)}$ decrease from 85.2 K ($x = 0.02$) to 64.4 K ($x = 0.10$) as more Zn dopant is added into the Ca side of the sample.

Figs 5 to 8 show the plot of the thermal diffusivity values versus dopant composition for $Bi_2Pb_{0.6}Sr_2Ca_{2-x}Ba_xCu_3O_\delta$ ($x = 0.02$–0.10), $Bi_2Pb_{0.6}Sr_2Ca_{2-x}V_xCu_3O_\delta$ ($x = 0.05$–0.10), $Bi_2Pb_{0.6}Sr_2Ca_{2-x}Y_xCu_3O_\delta$ ($x = 0.02$–0.10) and $Bi_2Pb_{0.6}Sr_2Ca_{2-x}Sn_xCu_3O_\delta$ ($x = 0.05$–0.10) respectively. We note that, the measured thermal diffusivity values were in the range of (0.19–1.09) cm^2/s where it increases when increasing the dopant (Ba, V, Y and Sn) concentration in the system. It is noted that in Fig. 7, for samples $Bi_2Pb_{0.6}Sr_2Ca_{2-x}Y_xCu_3O_\delta$ ($x = 0.02$–0.10), the thermal diffusvity value at $x = 0.02$ is 0.22 cm^2/s. It increases with increasing dopant concentration until reaching a maximun at $x = 0.09$ ($\alpha =$ of 0.33 cm^2/s). Above $x = 0.09$, the thermal diffusivity tends to decrease to 0.30 cm^2/s at $x = 0.10$.

On the other hand, the doping effect at the Ca sites of sample $Bi_2Pb_{0.6}Sr_2Ca_{2-x}M_xCu_3O_\delta$, (M = Ba, V, Y and Sn) does not fovour the formation of high Tc phase. The behavior of $Tc_{(R=0)}$ in Figs 5–7 decrease with the increasing mole fraction x of the dopant.

Fig. 9 shows the summary of thermal diffusivity values as a function of dopant concentation for Zn, Ba, V, Y and Sn doped superconductor samples. In Fig. 10, we show the scnning electron microscope micrographs of $Bi_2Pb_{0.6}Sr_2Ca_{2-x}Ba_xCu_3O_\delta$ ($x = 0.06$) and $Bi_2Pb_{0.6}Sr_2Ca_{2-x}Zn_xCu_3O_\delta$ ($x = 0.06$) samples. The entire samples in this work exhibit a common feature of plate-like layer grains (2223 phase) randomly distributed homogeneous and less compact.

The XRD patterns for samples $Bi_2Pb_{0.6}Sr_2Ca_{2-x}Ba_xCu_3O_\delta$ ($x = 0.02$–0.10) and $Bi_2Pb_{0.6}Sr_2Ca_{2-x}Zn_xCu_3O_\delta$ ($x = 0.02$–0.10) are shown in Figs 11 and 12. Peaks belonging to 2223 phase are indicated by $H(hkl)$ and for 2212 phase are indicated by $L(hkl)$. The volume fraction of the 2223 phase in the $Bi_2Pb_{0.6}Sr_2Ca_{2-x}Ba_xCu_3O_\delta$ decrease form 84% to 70% as Ba doping increases from $x = 0.02$ to $x = 0.10$. However, the volume fraction of the 2223 phase of the $Bi_2Pb_{0.6}Sr_2Ca_{2-x}Zn_xCu_3O_\delta$ samples varies from 40% to 60%. Similar results were obtained for other samples.

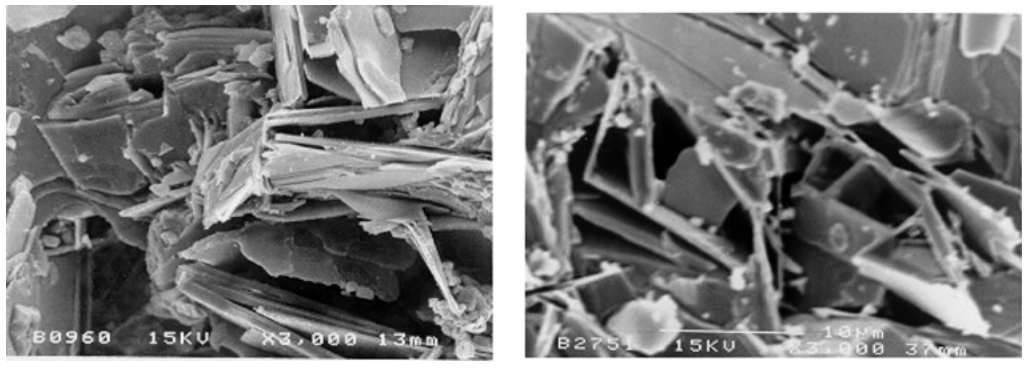

(a) (b)

Figure 10 SEM micrographs of (a) $Bi_2Pb_{0.6}Sr_2Ca_{2-x}Ba_xCu_3O_\delta$ ($x = 0.06$) and (b) $Bi_2Pb_{0.6}Sr_2Ca_{2-x}Zn_xCu_3O_\delta$ ($x = 0.06$) samples.

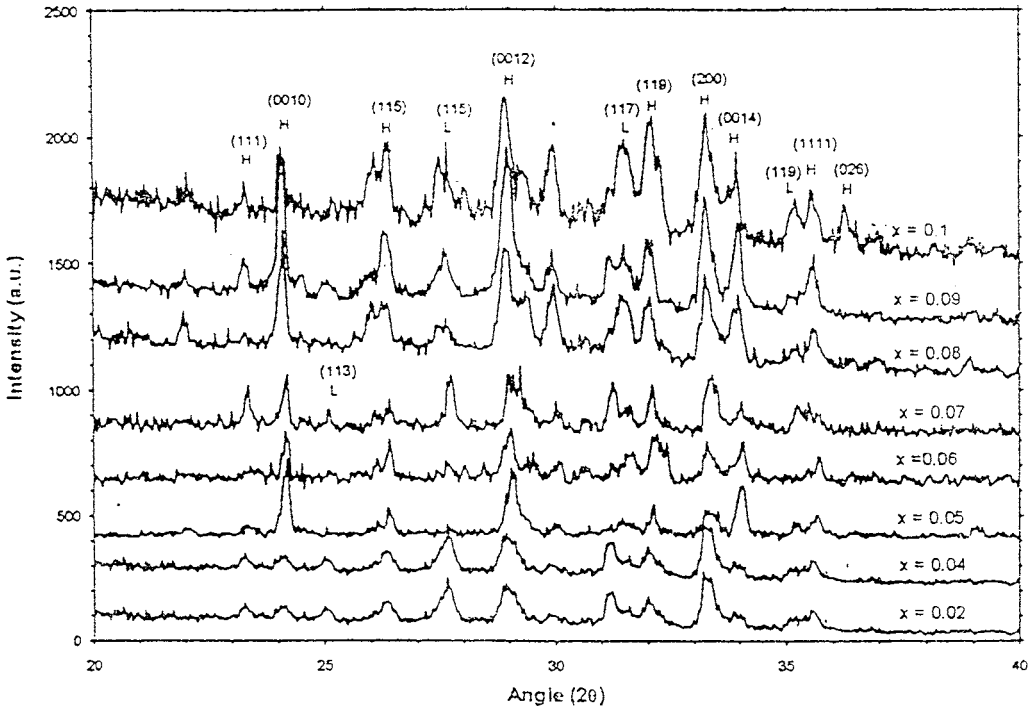

Figure 11 X-ray diffraction patterns of $Bi_2Pb_{0.6}Sr_2Ca_{2-x}Ba_xCu_3O_\delta$ ($x = 0.02$–0.10) samples.

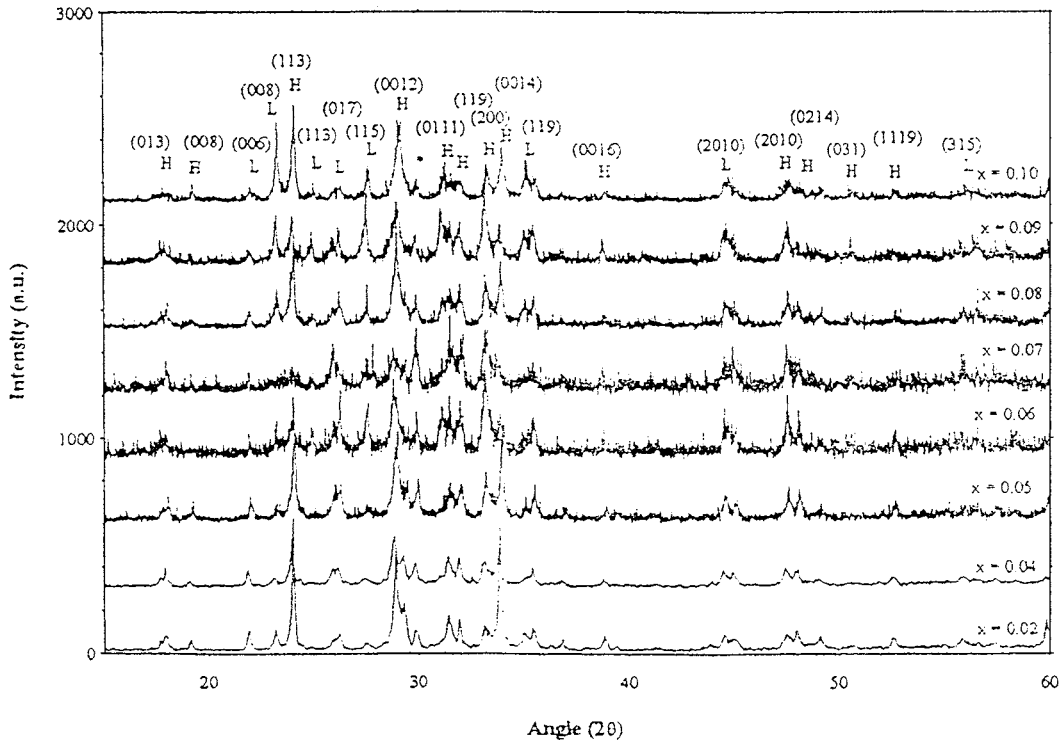

Figure 12 X-ray diffraction patterns of $Bi_2Pb_{0.6}Sr_2Ca_{2-x}Zn_xCu_3O_\delta$ ($x = 0.02$–0.10) samples.

4. Conclusion

It has been shown that by using the simple open photoacoustic cell technique, the thermal diffusvity for $Bi_2Pb_{0.6}Sr_2Ca_{2-x}M_xCu_3O_\delta$, (where M = Zn, Ba, V, Y and Sn and $x = 0.02$–0.10) samples were obtained. The measured thermal diffusivity value was found to be very dependent on the dopant atom and dopant concentration. When Zn doping at the Ca sites in the $Bi_2Pb_{0.6}Sr_2Ca_{2-x}Zn_xCu_3O_\delta$ system, the measured thermal diffusivity decrease with the increasing of Zn content. However, the thermal diffusivity values increase with the increasing of Ba, V, Y and Sn dopant in the $Bi_2Pb_{0.6}Sr_2Ca_{2-x}M_xCu_3O_\delta$ (M = Ba, V, Y and Sn) system. It is seen that, for dopant concentration, $x > 0.04$, the Ba doped sample gives higher thermal diffusivity value than other dopant in the superconduting system.

Acknowledgments

We thank the Malaysian Government and Universiti Putra Malaysia for research support through IRPA 09-02-04-0065 (51328) and Pasca (CYJF and TEP).

References

1. S. A. HALIM, S. B. MOHAMED, A. HASHIM and H. A. A. SIDEK, *Solid State Science and Technology* **6**(1) (1998) 1.
2. S. A. HALIM, S. B. MOHAMED, H. AZHAN, S. A. KHAWALDEH and H. A. A. SIDEK, *Physica* C (1990) 78.
3. S. B. MOHAMED, PhD thesis, Universiti Putra Malaysia, Malaysia, 1999.
4. J. C. DE LIMA, N. CELLA and L. C. M. MIRANDA, *Physical Rev.* B **46**(21) (1992) 14186.
5. S. O. FERREIRA, A. C. YING, I. N. BANDEIRA and L. C. M. MIRANDA, *Physical Rev.* B **39**(11) (1989) 7969.
6. M. V. MARQUEZINI, N. CELLA, A. M. MANSANARES, H. VARGAS and L. C. M. MIRANDA, *Meas. Sci. Technol.* **2** (1991) 398.
7. A. ROSENCWAIG and G. GERSHO, *J. Appl. Phys.* **47**(1) (1976) 64.
8. A. P. NETA, N. F. VARGAS and L. C. M. MIRANDA, *Physical Review* B **40**(6) (1989) 3924.
9. J. C. MURPHY, L. C. AAMODT and J. W. M. SPICER, "Principles & Perspectives of Photothermal & Photoacoustic Phenomena" (Elservier, New York, 1992).
10. W. M. MAT YUNUS, C. Y. J. FANNY, I. V. GROZESCU, A. ZAKARIA, Z. A. TALIB and M. M. MOKSIN, *Acta Physica Sinica* **8** (1999) S241.
11. C. Y. J. FANNY, W. M. MAT YUNUS, M. M. MOKSIN and S. A. HALIM, *J. Solid St. Sci. and Technol. Letters* **6**(2) (1999) 15.
12. L. F. PERONDI and L. C. M. MIRANDA, *J. Appl. Phys.* **62**(77) (1987) 2955.
13. A. C. R. DA COSTA and A. F. SIQUEIRA, *J. Appl. Phys.* **80**(10) (1996) 5579.

Received 14 June 2000
and accepted 1 October 2001